Experimental function estimation from quantum phase measurements

Ilaria Gianani,[1,*] Francesco Albarelli,[2] Valeria Cimini,[1] and Marco Barbieri[1,3]
[1]*Dipartimento di Scienze, Universitá degli Studi Roma Tre, Via della Vasca Navale 84, 00146 Rome, Italy*
[2]*Faculty of Physics, University of Warsaw, Pasteura 5, PL-02-093 Warszawa, Poland*
[3]*Istituto Nazionale di Ottica-CNR, Largo Enrico Fermi 6, 50125 Florence, Italy*

(Received 29 September 2020; revised 8 March 2021; accepted 17 March 2021; published 2 April 2021)

Characterizing and analyzing a system often requires learning an unknown function, such as the response of a system or the profile of a field. The standard approach is to opportunely sample the function at fiducial points and then interpolate. When the quantity of interest is embodied in physical objects accessible with quantum-enhanced measurements, it becomes relevant to investigate how to transfer this advantage from the individual sampled points to the estimation of the whole function. In this article we report the experimental quantum-enhanced function estimation of the optical response of a liquid crystal. Our results illustrate that optimizing the employment of the resources is not as straightforward as it may appear at a first glance: Quantum advantage becomes substantial only past a sampling density that depends on the interpolation method, and on the function at hand. Our results show how quantum resources should successfully be employed to access the rich information contained in continuous signals.

DOI: 10.1103/PhysRevA.103.042602

I. INTRODUCTION

In the quest for superior quantum technology, the development of sensors showing a palpable advantage has reached the state of solid demonstrations. The basic operations allowing for enhancement in precise measurements have indisputably been validated in photonics [1–4] and field sensing [5,6], realizing the promises of quantum metrology [7–10]. Current development is aiming, on one hand, at consolidating the technological readiness [11,12], on the other hand, at exploring new paradigms, based on the results attained so far.

Quantum sensors have been conceived as tools to inspect systems as their conditions are modified. When these changes are imparted by the variation of an external field, the sensing problem is intimately related to a key problem in physics, viz. determining the response function of the system. The experimental learning of the response function of a system is rooted in the evaluation of punctual fiducial response and interpolation to access prediction at arbitrary values. Obtaining an advantage in estimating the response function, certainly relies on the enhanced precision arising from measuring individual fiducial points by means of quantum resources. However, this improvement is unprofitable unless the sampling is sufficiently dense for the interpolation to be meaningful. These concepts have recently been addressed in Ref. [13] for what concerns the theoretical aspects. This combination of basic sensing to deliver a more complex result bears resemblance to the work flow in computing: Once elementary operations are mastered, these are then combined to deliver more elaborated capabilities.

In quantum photonics, phase estimation can indeed serve as such a primary element. Combining several phase estimation routines has lead to addressing novel problems, notably phase tracking [14–16]. This represents an instance of multiple phase estimation [17–21] with the difference that joint measurability of the different parameters has a limited interest. In this article, we implement quantum function estimation in a photonic experiment. The phase response of a liquid crystal to a voltage has been estimated by employing both quantum and classical resources, providing evidence of the superiority of the former strategy. We show that quantum enhancement is attained only if resources are cleverly distributed. An unconditional advantage could be obtained within the current technological effort [22], provided that sensors are used accounting for both the uncertainty on measured points, and the issue of interpolating between them.

The inclusion of function estimation in the toolkit of quantum metrology opens up unexplored opportunities for quantum enhancement in important problems, such as evaluating time-dependent signals and mapping fields [23–33]. Our paper emphasizes how quantum resources should successfully be employed to access the rich information contained in continuous signals, thus, laying the ground for the inclusion of quantum estimation in functional data analysis [34,35] in the near future.

II. EXPERIMENTAL RESULTS

A. Function estimation from phase measurements

Function estimation is formally an infinite-dimensional generalization of multiparameter estimation, which itself presents unique challenges in the quantum regime when the parameters are estimated simultaneously [2,36–40]. However, when the parameters can be considered statistically independent as we will assume in this paper, the advanced concepts and tools of multiparameter quantum metrology are not needed in full.

*ilaria.gianani@uniroma3.it

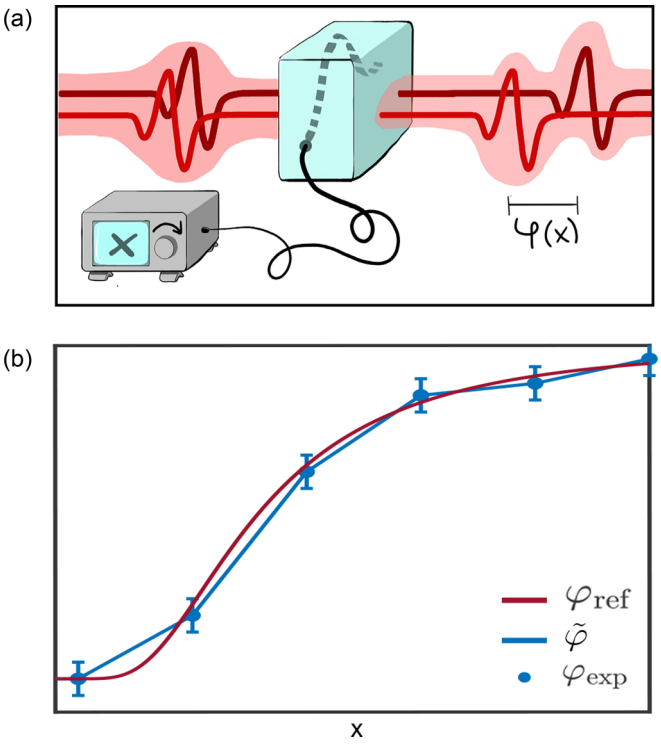

FIG. 1. Conceptual scheme of function estimation. (a) The optical response of a system to an applied voltage x is captured as the phase $\varphi(x)$ introduced between the polarization components aligned along the two optical axes. This phase is estimated at different values of x with suitably prepared light probes. (b) The experiment yields a function $\tilde{\varphi}(x)$ being an estimator of the actual response $\varphi(x)$, based on a set of fiducial points to which a statistical error is associated due to the limited amount of resources per point adopted.

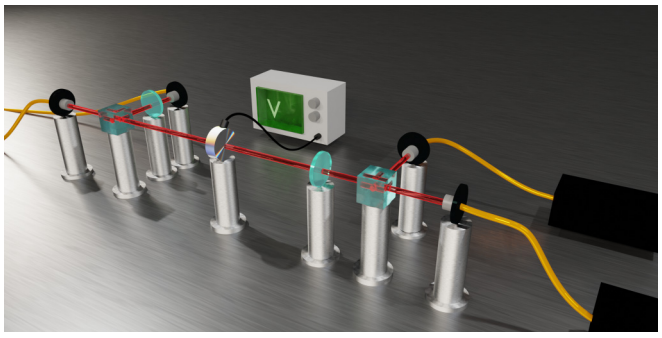

FIG. 2. Experimental setup. A CW diode laser at 405 nm pumps a 3-mm β-barium borate (BBO) crystal cut for noncollinear type-I phase matching, generating via SPDC two degenerate photons at 810 nm. The laser power is set to 50 mW for the reference measurement and to 6 and 13 mW, respectively, for the measurements at $N_r = 800$ an $N_r = 3800$. The two modes are then selected through interference filters with FWHM = 7.3 nm and single-mode fibers. For the NOON measurements, the polarization of one mode is rotated by means of a half-wave plate (HWP), and the two photons are then overlapped on the same spatial mode using a PBS, generating NOON states in the diagonal polarization basis. The two photons are then sent through the liquid-crystal device which alters the relative phase between the two modes according to the applied voltage. A projective measurement is performed by means of a a second HWP and PBS. For the individual photon measurements, the $|H\rangle$ polarized photon is still sent through the same setup, whereas the other is directly coupled to the detector for heralding. The output modes of the interferometer are coupled to single-mode fibers and sent to two avalanche photodiodes (APDs) for detection. The acquisition time is set to 3 s for the reference measurement and to 0.5 s for the two measurements at lower N_r. Coincidences are recorded by means of a field programmable gate array (FPGA).

Most of the literature on quantum function estimation is focused on the estimation of time-dependent signals with quantum probes both for deterministic functions and stochastic processes [23,26]. Here, we follow the analysis of Ref. [13], which is not specific to functions in the time domain and in which few and weak assumptions on the function are made.

Consider a system whose response function to an applied signal x is indeed a phase $\varphi(x)$ [Fig. 1(a)]. Different quantum-enhanced strategies can be envisaged to estimate the function $\varphi(x)$ [13]. In this paper, we perform independent experiments for each point x_i to obtain estimates of the fiducial values $\tilde{\varphi}_i = \tilde{\varphi}(x_i)$, treating each estimation as a single parameter problem. This simple strategy represents the most common instance in practical applications. If enough experimental values $\varphi_{\text{exp}}(x)$ are collected as fiducial references, one can interpolate them in order to obtain an estimate $\tilde{\varphi}(x)$ of the entire function over a given range $[0, L]$ [Fig. 1(b)]. The accuracy on $\tilde{\varphi}(x)$ will depend on the interpolation method, on the number N_s and the positions of the points x_i at which the signal is sampled, and on the uncertainty on the measured values. We remark that this approach is nonparametric since no functional form (with a *finite* number of unknown parameters) is assumed *a priori* for the function.

When a fixed amount of resources (i.e., the total number of photons) are allocated, they need to be optimally deployed, taking into account these contrasting error sources. These considerations are important already at the classical level, but crucially they also impact the possibility of attaining an overall quantum advantage. For any given value of x, quantum-enhanced phase estimation guarantees improved precision *punctually* on the system response. By leveraging on this ameliorated performance, the estimation of the whole function can also be improved.

The most straightforward implication is that, for fixed resources at each reference point, the errors on the punctual estimates will decrease when using quantum light. There is, however, a subtler effect: For a given amount of total resources, and given acceptable statistical uncertainty on the fiducial points, quantum light allows to increase the sampling density. We exploit the setup presented in (Fig. 3) to illustrate these mechanisms.

A scenario for which this approach is relevant is described in Fig. 2. We consider the response function of a liquid crystal device to an applied voltage which can be controlled and swept across the range [0, 3] V as the birefringent phase associated with its optical axes. We set the crystal so that the voltage-induced fast and slow axes are oriented along the diagonal (D) and antidiagonal (A) polarizations. This phase is estimated based on measurements on individual photons, providing the classical limit, and NOON states,

exhibiting quantum advantage. These are generated with a noncollinear type-I spontaneous parametric downconversion (SPDC) source. Individual photons are heralded on one of the modes of the SPDC and are prepared in the horizontal polarization, i.e., the superposition of D and A: $|\psi_1\rangle = (|1\rangle_D|0\rangle_A + |0\rangle_D|1\rangle_A)/\sqrt{2}$. In order to produce the NOON states, we make use of both photons from SPDC which are superposed with orthogonal polarizations on a polarizing beam splitter (PBS). This operation prepares them in a NOON state in the diagonal basis: $|\psi_2\rangle = (|2\rangle_D|0\rangle_A + |0\rangle_D|2\rangle_A)/\sqrt{2}$. The relative phase is accumulated twice as fast in state $|\psi_2\rangle$ than in $|\psi_1\rangle$, resulting in superior sensitivity. A projective measurement is performed by means of a HWP and PBS. We record the coincidence counts corresponding to the postselected outcome probabilities,

$$P_\theta[\varphi(x), v(x)] = \tfrac{1}{4}\{1 + v(x)\cos\, m[4\theta - 2\varphi(x)]\}, \qquad (1)$$

where $m = 1$ for $|\psi_1\rangle$ and $m = 2$ for $|\psi_2\rangle$. In this formula, v is the fringe visibility, and the HWP is set to $\theta = \{0, \pi/(8m), \pi/(4m), 3\pi/(8m)\}$. The impact of postselection on the Fisher information is detailed in Ref. [41].

For each voltage setting x_i, the corresponding value of the phase φ_i is retrieved by means of either $|\psi_1\rangle$ or $|\psi_2\rangle$ through a multiparameter Bayesian routine, which includes the *estimation* of the fringe visibility [41]. Although the estimated value of $v(x)$ is not used in the subsequent interpolation, such a multiparameter approach guarantees that the estimation of $\varphi(x)$ is unbiased and robust against the instabilities of the system, which might become significant due to the amount of time necessary to accumulate the signal and sampling required.

The parameters are calculated starting from the Bayesian probability defined as

$$P_B[\varphi(x), v(x)] = \mathcal{N}\prod_\theta P_\theta[\varphi(x), v(x)]^{n_\theta} P_A[\varphi(x), v(x)], \quad (2)$$

where $\mathcal{N}$ is a normalization constant and n_θ are the measured coincidences for the θth projection. The *a priori* probability distribution P_A is chosen a step function centered around the values directly estimated from the data for the sake of computational efficiency. The first moments $\varphi_B(x)$, $v_B(x)$, and the second moments $\Delta^2\varphi_B(x)$, $\Delta^2 v_B(x)$ of the marginal distributions yield the desired quantities.

We obtained phase estimates at $N_s^{\max} = 100$ equally spaced points in the interval $[0, L]$. The amount of resources N_r employed for each punctual estimation is given by the number of photons in the state times the number of repetitions of the measurement and has been fixed at $N_r = 800$ and $N_r = 3800$ both for NOON and single-photon states.

B. Benchmarking error in function estimation

This data collection does not complete the estimation procedure: These phase values are then employed to obtain estimates of the function $\tilde{\varphi}(x)$ for arbitrary values, using two different strategies, viz. linear and nearest-neighbor interpolation. These are commonly employed choices depending on how regular the function is assumed to be.

The associated *global* error can then be quantified by [42]

$$\delta_0^2 = \frac{1}{L}\mathbb{E}\left[\int |\varphi(x) - \tilde{\varphi}(x)|^2 dx\right], \qquad (3)$$

which is the average quadratic deviation over the whole variable range. This can essentially be considered as a continuous analog of the trace of the mean-square error matrix, commonly chosen as the figure of merit in multiparameter estimation.

As a matter of fact, the true function $\varphi(x)$ is unknown, making the error (3) experimentally inaccessible. A measurable proxy can be obtained by assessing values of $\varphi(x)$ at much denser sampling and much lower statistical uncertainty than the points used in the experiment: These are identifiable for all practical purposes with the true values of the function. We measure the reference phase $\varphi_{\rm ref}(x)$, using NOON states, acquiring $N_s^{\rm ref} = 500$ sampling points adopting $N_r \simeq 60 \times 10^3$ resources for each fiducial point sampled. The corresponding phase measurements are shown in Fig. 3. Consequently, the error in (3) can be approximated by a sum over a discrete set of values of x, dictated by the sampling of the reference $\varphi_{\rm ref}(x)$,

$$\delta^2 = \frac{1}{L}\sum_{x=0}^{L}\mathbb{E}[|\tilde{\varphi}(x) - \varphi_{\rm ref}(x)|^2]\Delta x_{\rm ref}, \qquad (4)$$

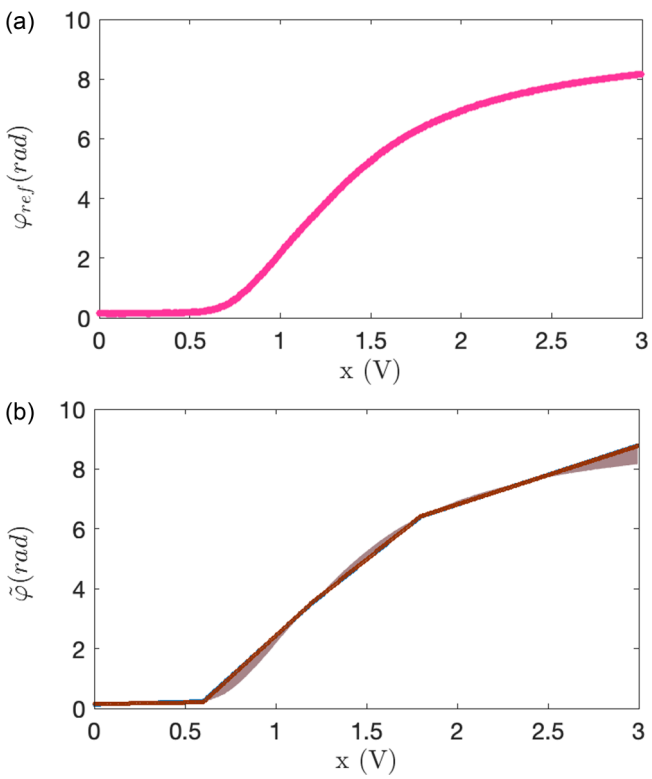

FIG. 3. Response function measurement. (a) Birefringent reference phase $\varphi_{\rm ref}(x)$ imparted by the liquid-crystal device at different voltage values measured with NOON states with $N_s = 500$ ($\Delta x = 0.006$ V) and $N_r \simeq 60 \times 10^3$, estimated via a multiparameter Bayesian approach as discussed in the text. In the graph the errors are smaller than the datapoints. (b) Example of the interpolated estimated response function $\tilde{\varphi}(x)$ for $N_s = 5$ and $N_r = 3800$. The shaded area corresponds to the difference $\Delta\tilde{\varphi}(x) = \varphi_{\rm ref}(x) - \tilde{\varphi}(x)$ for classical resources (red) and NOON states (blue). The complete overlap of the two curves, resulting in the brown colored area, shows that there is no difference at this sampling density in the estimation with quantum and classical resources.

where $\Delta x_{\rm ref}$ is the sampling resolution of the reference. This is the figure of merit we explored in our experiment. Different from the original proposal [13], we do not focus on showing the difference between a quantum and a classical scaling of the error with the number of photons: In fact, this is an asymptotic property which we cannot capture with our probe states.

For our experiment it is more relevant to investigate what happens as we increase the resolution N_s for a fixed level of uncertainty on the individual sampling points. This allows us to analyze independently the sources of error contributing to δ^2. For both strategies, function estimation is carried out as follows: For each estimated phase we select datapoints so to obtain subsets composed of a different value of sampling points N_s, up to $N_s^{\rm max} = 100$. For each subset we interpolate the points to match the sampling of the reference $N_s^{\rm ref}$ using the two methods introduced above. In performing this, we investigate the effect of increasing the density of the sampling for fixed resources N_r on the individual points. Therefore, a different amount of total resources $\mathbf{N} = N_r N_s$ is employed for distinct values of N_s.

An example of the reconstructed phase based on linear interpolation is presented in Fig. 3(b) for $N_s = 5$ to emphasize the effect of limited sampling. The shaded areas correspond to the uncertainty regions, which are the wider the further the region from a sampled point. We can assess how the interpolation error behaves when increasing the sample density in Fig. 4 that shows a closeup of the same curve of Fig. 3(b). Increasing N_s does lead to an improved reconstruction with the different performance between quantum and classical resources becoming evident only for denser sampling.

These considerations are captured by the error δ^2 which we show in Fig. 5 both for linear and nearest-neighbor interpolations.

The related uncertainties are obtained performing a Monte Carlo routine as follows: 500 sets of the estimated phase values are generated by adding a random Gaussian distributed error with variance $\Delta^2\varphi_B(x)$ to the estimated values $\varphi_B(x)$. For each set of phases, the resampling and interpolation procedures are then performed as described in the main text, and the error δ^2 is calculated. The error on δ^2 is, hence, obtained from the standard deviation over the 500 repetitions of δ^2.

As a consistency check we also determined the error δ^2 that would be obtained by an ideal phase estimation at the fiducial points. To do so, we have employed the measured $\varphi_{\rm ref}(x)$ both as a reference and as a set of data from which we have selected N_s sampling points. To simulate experimental data, we have performed a Monte Carlo routine adding to the sampled points a random Gaussian distributed error with variance dictated by the Cramér-Rao bound: $\varepsilon_i^2 = 1/N_r F_i$, where F_i is the Fisher information for the classical and quantum measurements, which reads [41]

$$F_c = \frac{2v(x)^2}{4 - v(x)^2[1 - \cos\, 4\varphi(x)]}$$

$$F_q = \frac{8v(x)^2}{4 - v(x)^2[1 - \cos\, 8\varphi(x)]}.$$

We have then performed the interpolation procedure as described for the actual experimental data. The obtained simulated mean values are shown as dotted lines in Fig. 5.

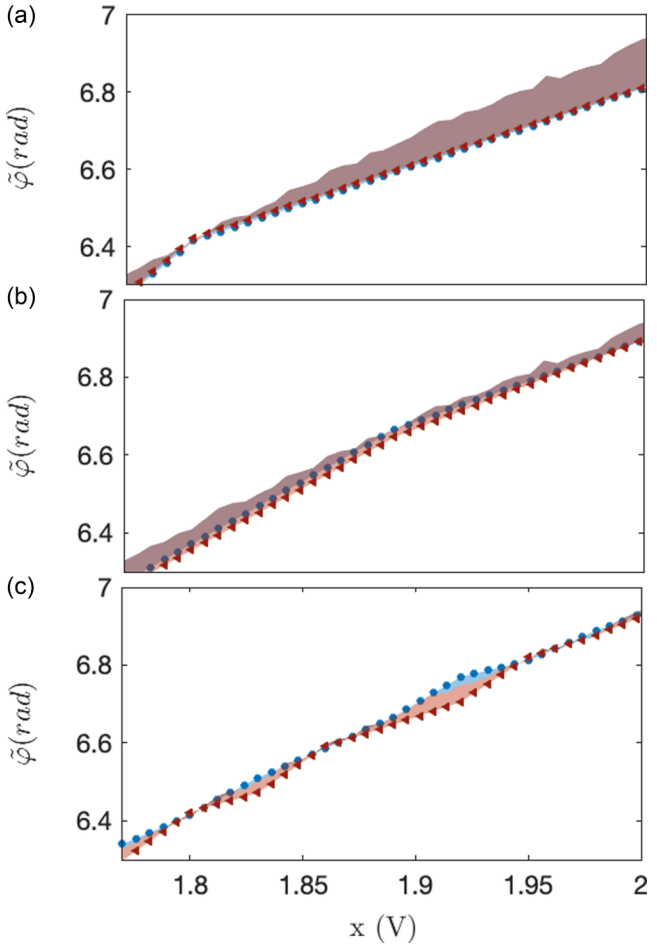

FIG. 4. Interpolation error. The three panels show a portion of the interpolated estimated response function $\tilde{\varphi}$ obtained with classical (red triangles) and quantum (blue circles) resources with $N_r = 3800$ for three different sampling densities: (a) $N_s = 5$, (b) $N_s = 10$, and (c) $N_s = 100$. The shaded area corresponds to the difference $\Delta\tilde{\varphi}(x) = \varphi_{\rm ref}(x) - \tilde{\varphi}(x)$ for classical resources (red) and NOON states (blue). The brown shade indicates where the two contributions overlap.

For the nearest-neighbor [panels (a) and (b)], the primary source of error up to $N_s = 50$ comes from the interpolation, rather than from the statistical uncertainties. Therefore, if more resources are available, they would be more conveniently used to increase the sampling density, rather than improving the significance of the individual points. However, for denser sampling the advantage of quantum light becomes relevant: Resources can be allocated to improve the punctual uncertainties. This analysis mirrors the one in the proposal [13], which considered this same interpolation method.

For the linear interpolation [panels (c) and (d)], fewer points are needed in order to achieve the same accuracy on the estimation of the whole function. The improvement linked to the use of quantum resources becomes relevant earlier but eventually saturates due to the statistical error. In these panels, the same Monte Carlo methods have been employed to quantify the uncertainties on δ^2 as well as the expected values.

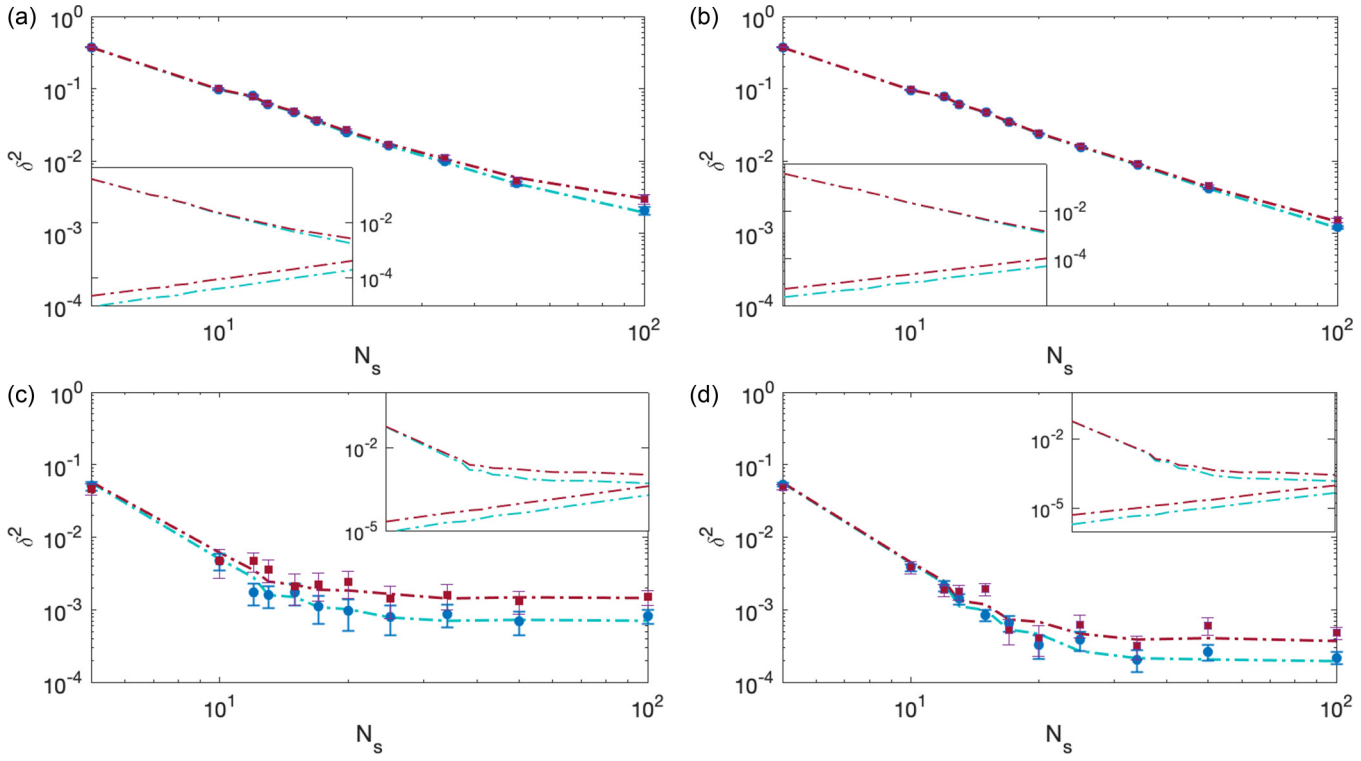

FIG. 5. Function estimation. Simulated (dotted lines) and measured error δ^2 as a function of the number of sampled points N_s with NOON states (blue circles) and individual photons (red squares) probes for (a) $N_r = 800$ for nearest-neighbor interpolation, (b) $N_r = 3800$ for nearest-neighbor interpolation, (c) $N_r = 800$ for linear interpolation, and (d) $N_r = 3800$ for linear interpolation. The errors are compatible with what expected from the simulations performed at the Cramér-Rao bound. The insets show, on the same scales, the two contributions to δ^2: The one arising from the statistical error on the fiducial points, which increases with the number of sampling points, and the contribution due to the interpolation on the remaining points, which instead decreases with the sampling density.

These results illustrate how there are two distinct contributions to the overall function error δ^2, which are captured by the insets in each panel of Fig. 5 both for classical (red) and quantum (blue) resources: The one given by the statistical errors on the fiducial points and that given by the errors on the interpolated points. As discussed earlier, employing quantum resources always guarantees a *punctual* advantage on the sampling points. This contribution to the error δ^2 will, thus, increase with the sampling density, and ultimately will determine the overall minimum error achievable. On the other hand, increasing the sampling density will drastically affect the interpolation error. Remarkably, having a quantum enhancement on the sampling points will also benefit the interpolation error as also shown in Fig. 4.

III. ADDITIONAL SIMULATIONS

The inspection of our error budgeting highlights how careful consideration must be given when distributing the available resources to either diminishing the punctual uncertainties or increasing the resolution. These two contributions are kept independent only at the cost of investing more resources with the sampling density as we could in our experiment. On the other hand, whenever an upper limit to the level of illumination is set to **N** photons overall, there may exist an interplay between the statistical and the interpolation errors contributing to the overall uncertainty on the function.

We estimated how severe this trade-off is by performing additional simulations with a fixed number of total resources **N**: When N_s increases, the number of resources per punctual estimation will diminish. We have used the same response function employed in the experiment with the same details discussed above but for fixed $\mathbf{N} = 10^3$, 10^4, 2×10^4, and 5×10^4. The results are shown in Fig. 6 and prove that when the resources are limited there is an optimal value of N_s, confirming the necessity of apportioning the total resources wisely. These conditions are eased when **N** exceeds 2×10^4 for our example, provided that the sampling exceeds $N_s \simeq 50$.

A different consideration pertains the impact of the function itself, in particular, its gradient over the investigated region on the sampling required for a quantum advantage. We have selected three numerical examples with varying modulation as reported in Fig. 7. For each response function we evaluate the error δ^2 as discussed earlier using the same interpolation methods as before (linear and nearest neighbor) with fixed $N_r = 1000$ both for NOON and single-photon states. For the exponential response function, the enhancement is visible even at very small N_s for the low-frequency sine function the range of N_s considered is sufficient to reach the stage in which the error given by the interpolation is smaller than that due to the statistics (either classical or quantum), similar to the response function in our experiment. With the high-frequency sine function, the interpolation error at the maximum N_s considered is comparable to the statistical error for the linear

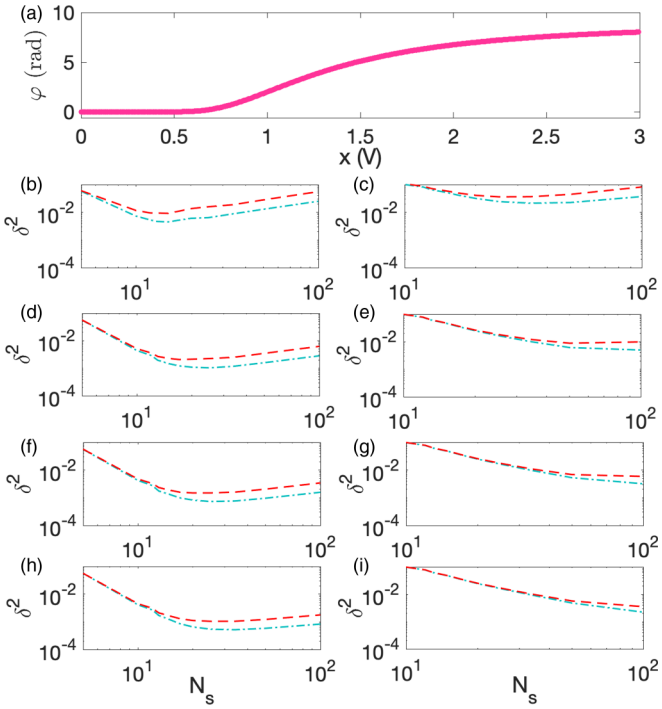

FIG. 6. Simulated error δ^2 for the LC response function (a). The error δ^2 is evaluated with linear (left column) and nearest-neighbor (right column) interpolations with NOON states (light blue, "-.") and individual photons (red, "- -") probes for (b) and (c) $\mathbf{N} = 10^3$, (d) and (e) $\mathbf{N} = 10^4$, (f) and (g) $\mathbf{N} = 2 \times 10^4$, and (h) and (i) $\mathbf{N} = 5 \times 10^4$.

interpolation, whereas still higher for the nearest-neighbor interpolation: A denser sampling would be needed to appreciate the quantum enhancement.

IV. CONCLUSIONS

To conclude, we have a presented a proof-of-principle estimation of a simple function based upon photonic metrology. In this experiment we highlight the crucial interplay between statistical and interpolation errors, which becomes evident already at relatively low sampling densities. Increasing N_s can improve the estimation only up to a limit in which the statistical uncertainty on the individual points becomes the predominant source as determined by the complexity of the function. Quantum strategies are only beneficial once this level is attained.

Different strategies might be optimal for other estimation tasks involving an unknown function. For example, one might be interested to estimate only a few scalar functionals. This kind of problem is better approached in the framework of semiparametric estimation, recently generalized and applied to the quantum domain [43–45].

In more applied scenarios, such as probing of the response of biological systems [46], more complicated functions will be sampled, and the advantage of punctual reduced statistical uncertainty will likely become manifest at higher sampling densities. Therefore, to minimize the overall error (3) it will be fundamental to take into account the interpolation, as we have shown, to make a judicious choice about the allocation of the resources.

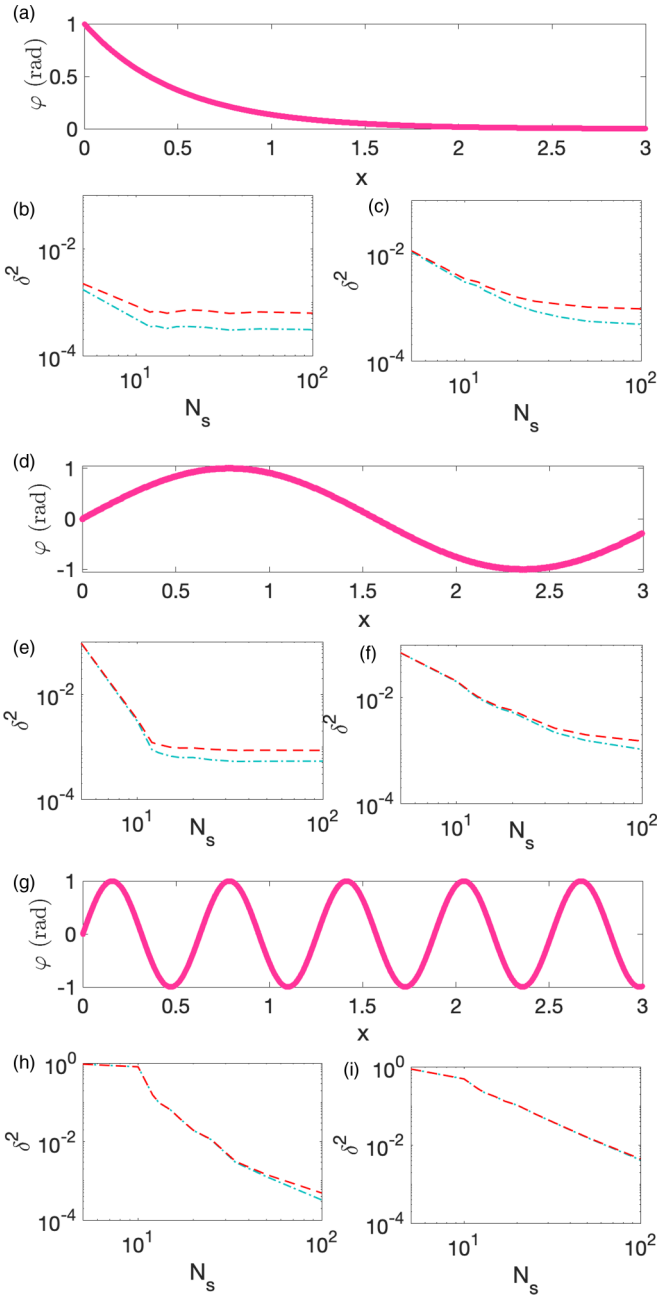

FIG. 7. (a) Slow exponential decay, (d) low-frequency sine response function, and (g) high-frequency sine response function. (b), (e), and (h) Simulated error δ^2 as a function of the number of sampled points N_s with NOON states (light blue, "-.") and individual photons (red, "- -") probes for linear interpolation, and (c), (f), and (i) nearest-neighbor interpolation.

As the interest of quantum metrology moves towards more elaborated problems, functional data analysis may become a subject for new studies. Here, the random variable of interest is indeed a function [34,35]; in the standard approach its sampling is taken sufficiently dense, but techniques reaching out to the sparse case have also been discussed [47]. Quantum-enhanced strategies may provide a way of mitigating the limitations due to sparse sampling, whereas not compromising precision for given resources. Overall, the interplay and the

connections between functional data analysis and quantum metrology remain largely unexplored at present.

ACKNOWLEDGMENTS

We thank F. Sciarrino for the loan of scientific equipment, A. Verna, and R. Demkowicz-Dobrzański for valuable discussions, and M. De Seta, L. Di Gaspare, and I. Agha for useful comments. This work was supported by the H2020 FET Open Project STORMYTUNE (Grant Agreement No. 899587). I.G. was supported by Ministero dell'Istruzione, dell'Universitá e della Ricerca Grant of Excellence Departments (ARTICOLO 1, COMMI 314-337, LEGGE 232/2016). F.A. acknowledges financial support from the National Science Center (Poland) Grant No. 2016/22/E/ST2/00559.

[1] E. Polino, M. Valeri, N. Spagnolo, and F. Sciarrino, Photonic quantum metrology, AVS Quantum Sci. **2**, 024703 (2020).

[2] F. Albarelli, M. Barbieri, M. G. Genoni, and I. Gianani, A perspective on multiparameter quantum metrology: From theoretical tools to applications in quantum imaging, Phys. Lett. A **384**, 126311 (2020).

[3] S. Pirandola, B. R. Bardhan, T. Gehring, C. Weedbrook, and S. Lloyd, Advances in photonic quantum sensing, Nat. Photonics **12**, 724 (2018).

[4] R. Demkowicz-Dobrzański, M. Jarzyna, and J. Kołodyński, Chapter 4—Quantum Limits in Optical Interferometry, Prog. Opt. **60**, 345 (2015).

[5] L. Pezzè, A. Smerzi, M. K. Oberthaler, R. Schmied, and P. Treutlein, Quantum metrology with nonclassical states of atomic ensembles, Rev. Mod. Phys. **90**, 035005 (2018).

[6] C. L. Degen, F. Reinhard, and P. Cappellaro, Quantum sensing, Rev. Mod. Phys. **89**, 035002 (2017).

[7] V. Giovannetti, S. Lloyd, and L. Maccone, Quantum-enhanced measurements: Beating the standard quantum limit, Science **306**, 1330 (2004).

[8] V. Giovannetti, S. Lloyd, and L. Maccone, Quantum Metrology, Phys. Rev. Lett. **96**, 010401 (2006).

[9] M. G. A. Paris, Quantum estimation for quantum technology, Int. J. Quantum Inf. **07**, 125 (2009).

[10] H. Lee, P. Kok, and J. P. Dowling, A quantum Rosetta stone for interferometry, J. Mod. Opt. **49**, 2325 (2002).

[11] M. Tse, H. Yu, N. Kijbunchoo, A. Fernandez-Galiana, P. Dupej, L. Barsotti, C. D. Blair, D. D. Brown, S. E. Dwyer, A. Effler *et al.*, Quantum-Enhanced Advanced LIGO Detectors in the Era of Gravitational-Wave Astronomy, Phys. Rev. Lett. **123**, 231107 (2019).

[12] F. Acernese, M. Agathos, L. Aiello, A. Allocca, A. Amato, S. Ansoldi, S. Antier, M. Arène, N. Arnaud, S. Ascenzi *et al.*, Increasing the Astrophysical Reach of the Advanced Virgo Detector via the Application of Squeezed Vacuum States of Light, Phys. Rev. Lett. **123**, 231108 (2019).

[13] N. Kura and M. Ueda, Standard Quantum Limit and Heisenberg Limit in Function Estimation, Phys. Rev. Lett. **124**, 010507 (2020).

[14] T. A. Wheatley, D. W. Berry, H. Yonezawa, D. Nakane, H. Arao, D. T. Pope, T. C. Ralph, H. M. Wiseman, A. Furusawa, and E. H. Huntington, Adaptive Optical Phase Estimation Using Time-Symmetric Quantum Smoothing, Phys. Rev. Lett. **104**, 093601 (2010).

[15] H. Yonezawa, D. Nakane, T. A. Wheatley, K. Iwasawa, S. Takeda, H. Arao, K. Ohki, K. Tsumura, D. W. Berry, T. C. Ralph, H. M. Wiseman, E. H. Huntington, and A. Furusawa, Quantum-enhanced optical-phase tracking, Science **337**, 1514 (2012).

[16] V. Cimini, M. Mellini, G. Rampioni, M. Sbroscia, L. Leoni, M. Barbieri, and I. Gianani, Adaptive tracking of enzymatic reactions with quantum light, Opt. Express **27**, 35245 (2019).

[17] P. C. Humphreys, M. Barbieri, A. Datta, and I. A. Walmsley, Quantum Enhanced Multiple Phase Estimation, Phys. Rev. Lett. **111**, 070403 (2013).

[18] L. Pezzè, M. A. Ciampini, N. Spagnolo, P. C. Humphreys, A. Datta, I. A. Walmsley, M. Barbieri, F. Sciarrino, and A. Smerzi, Optimal Measurements for Simultaneous Quantum Estimation of Multiple Phases, Phys. Rev. Lett. **119**, 130504 (2017).

[19] E. Polino, M. Riva, M. Valeri, R. Silvestri, G. Corrielli, A. Crespi, N. Spagnolo, R. Osellame, and F. Sciarrino, Experimental multiphase estimation on a chip, Optica **6**, 288 (2019).

[20] M. Valeri, E. Polino, D. Poderini, I. Gianani, G. Corrielli, A. Crespi, R. Osellame, N. Spagnolo, and F. Sciarrino, Experimental adaptive Bayesian estimation of multiple phases with limited data, npj Quantum Inf. **6**, 92 (2020).

[21] V. Cimini, E. Polino, M. Valeri, I. Gianani, N. Spagnolo, G. Corrielli, A. Crespi, R. Osellame, M. Barbieri, and F. Sciarrino, Calibration of Multiparameter Sensors via Machine Learning at the Single-Photon Level, Phys. Rev. Appl. (to be published).

[22] S. Slussarenko, M. M. Weston, H. M. Chrzanowski, L. K. Shalm, V. B. Verma, S. W. Nam, and G. J. Pryde, Unconditional violation of the shot-noise limit in photonic quantum metrology, Nat. Photonics **11**, 700 (2017).

[23] M. Tsang, H. M. Wiseman, and C. M. Caves, Fundamental Quantum Limit to Waveform Estimation, Phys. Rev. Lett. **106**, 090401 (2011).

[24] V. Petersen and K. Mølmer, Estimation of fluctuating magnetic fields by an atomic magnetometer, Phys. Rev. A **74**, 043802 (2006).

[25] D. W. Berry, M. J. W. Hall, and H. M. Wiseman, Stochastic Heisenberg Limit: Optimal Estimation of a Fluctuating Phase, Phys. Rev. Lett. **111**, 113601 (2013).

[26] D. W. Berry, M. Tsang, M. J. W. Hall, and H. M. Wiseman, Quantum Bell-Ziv-Zakai Bounds and Heisenberg Limits for Waveform Estimation, Phys. Rev. X **5**, 031018 (2015).

[27] S. Ng, S. Z. Ang, T. A. Wheatley, H. Yonezawa, A. Furusawa, E. H. Huntington, and M. Tsang, Spectrum analysis with quantum dynamical systems, Phys. Rev. A **93**, 042121 (2016).

[28] T. Baumgratz and A. Datta, Quantum Enhanced Estimation of a Multidimensional Field, Phys. Rev. Lett. **116**, 030801 (2016).

[29] C. Bonato and D. W. Berry, Adaptive tracking of a time-varying field with a quantum sensor, Phys. Rev. A **95**, 052348 (2017).

[30] F. Martin Ciurana, G. Colangelo, L. Slodička, R. J. Sewell, and M. W. Mitchell, Entanglement-Enhanced Radio-Frequency

Field Detection and Waveform Sensing, Phys. Rev. Lett. **119**, 043603 (2017).

[31] K. T. Laverick, H. M. Wiseman, H. T. Dinani, and D. W. Berry, Adaptive estimation of a time-varying phase with coherent states: Smoothing can give an unbounded improvement over filtering, Phys. Rev. A **97**, 042334 (2018).

[32] R. Jiménez-Martínez, J. Kołodyński, C. Troullinou, V. G. Lucivero, J. Kong, and M. W. Mitchell, Signal Tracking Beyond the Time Resolution of an Atomic Sensor by Kalman Filtering, Phys. Rev. Lett. **120**, 040503 (2018).

[33] C. Zhang and K. Mølmer, Estimating a fluctuating magnetic field with a continuously monitored atomic ensemble, Phys. Rev. A **102**, 063716 (2020).

[34] J. O. Ramsay and B. W. Silverman, *Applied Functional Data Analysis* (Springer-Verlag, New York, 2002).

[35] J.-L. Wang, J.-M. Chiou, and H.-G. Müller, Functional Data Analysis, Annu. Rev. Stat. Its Appl. **3**, 257 (2016).

[36] M. Szczykulska, T. Baumgratz, and A. Datta, Multi-parameter quantum metrology, Adv. Phys.: X **1**, 621 (2016).

[37] J. Liu, H. Yuan, X.-M. Lu, and X. Wang, Quantum Fisher information matrix and multiparameter estimation, J. Phys. A: Math. Theor. **53**, 023001 (2020).

[38] R. Demkowicz-Dobrzański, W. Górecki, and M. Guţă, Multi-parameter estimation beyond quantum Fisher information, J. Phys. A: Math. Theor. **53**, 363001 (2020).

[39] Z. Hou, Y. Jin, H. Chen, J.-F. Tang, C.-J. Huang, H. Yuan, G.-Y. Xiang, C.-F. Li, and G.-C. Guo, "Super-Heisenberg" and Heisenberg Scalings Achieved Simultaneously in the Estimation of a Rotating Field, Phys. Rev. Lett. **126**, 070503 (2021).

[40] Z. Hou, J.-F. Tang, H. Chen, H. Yuan, G.-Y. Xiang, C.-F. Li, and G.-C. Guo, Zero–trade-off multiparameter quantum estimation via simultaneously saturating multiple heisenberg uncertainty relations, Sci. Adv. **7**, eabd2986 (2021).

[41] E. Roccia, V. Cimini, M. Sbroscia, I. Gianani, L. Ruggiero, L. Mancino, M. G. Genoni, M. A. Ricci, and M. Barbieri, Multiparameter approach to quantum phase estimation with limited visibility, Optica **5**, 1171 (2018).

[42] M. P. Wand and M. C. Jones, *Kernel Smoothing* (CRC, Boca Raton, FL, 1994).

[43] M. Tsang, F. Albarelli, and A. Datta, Quantum Semiparametric Estimation, Phys. Rev. X **10**, 031023 (2020).

[44] M. Tsang, Semiparametric estimation for incoherent optical imaging, Phys. Rev. Res. **1**, 033006 (2019).

[45] M. Tsang, Semiparametric bounds for subdiffraction incoherent optical imaging: A parametric-submodel approach, arXiv:2010.03518.

[46] M. A. Taylor and W. P. Bowen, Quantum metrology and its application in biology, Phys. Rep. **615**, 1 (2016).

[47] X. Zhang and J.-L. Wang, From sparse to dense functional data and beyond, Ann. Stat. **44**, 2281 (2016).